Neutron resonance spectroscopy: Ta

G. Hacken,* R. Werbin,* and J. Rainwater
Columbia University, New York, New York 10027
(Received 23 June 1977)

Results of high resolution neutron time of flight spectroscopy on natural tantalum (99.988% ^{181}Ta, $I^\pi = 7/2^+$) are presented for $l = 0$ resonances to 2025 eV. Values of E and $g\Gamma_n^0$ are presented for 431 resonances, in addition to the three resonances below 15 eV. A Bayes analysis suggests that no p wave levels have been included. The analysis used a multilevel Breit-Wigner shape fitting to the measured transmission curves for three different sample thicknesses. Doppler broadening and potential-resonance interference effects were included, plus some simulation of the experimental resolution effects. The analysis gives $\langle S \rangle = (4.17 \pm 0.04)$ eV for the mean level spacing, and $10^4 S_0 = (1.68 \pm 0.11)$ for the $l = 0$ strength function.

[NUCLEAR REACTIONS ^{181}Ta(n, total), E=15 to 2030 eV; deduced resonance E, $g\Gamma_n^0$, $\langle S \rangle$, S_0.]

I. INTRODUCTION

This is one of a series[1,2] of papers reporting the results of high resolution neutron time of flight spectroscopy measurements using the Columbia University Nevis synchrocyclotron as a pulsed neutron source. Natural metallic Ta samples were used which are 99.988% ^{181}Ta $[I^\pi = (\frac{7}{2})^+]$ so only one single odd A Ta isotope contributes. Since ^{181}Ta is near the peak of the $l=0$ strength function S_0 and a minimum of the $l=1$ strength function S_1, the observed resonances to a few keV neutron energy are essentially all $l=0$. The presently reported measurements are based on 202.05 m transmission measurements, of which the data from about 15 to 2030 eV have been analyzed. Level energies and $g\Gamma_n^0$ values are presented for 431 resonances to 2023 eV, excluding the three resonances below 20 eV. The present level parameter selections are based on fitting the measured neutron transmission T vs E curves for three different sample thicknesses, using a multilevel Breit-Wigner formalism, with some modification of the calculated T fit curves to partially simulate resolution effects.

The previous evaluations of Ta resonance parameters above 200 eV are all based on measurements using the Nevis synchrocyclotron. The first measurements by Desjardins *et al.*[3] used a 35 m flight path for self-indication measurements and gave parameters for 62 resonances in Ta to 330 eV. After our 200 m flight path had been constructed, occasional transmission measurements were made for Ta samples. Garg analyzed these data for resonance energies to 1400 eV and $g\Gamma_n^0$ values to 247 eV with the results presented in the 1966 edition of BNL-325. He subsequently reanalyzed this pre-1966 data for resonance energies and $g\Gamma_n^0$ values to 1400 eV. The resonance parameters given in the 1973 edition of BNL-325[4] above 250 eV are from that analysis, except that a number of his weakest resonances were omitted at the recommendation of Rahn after a preliminary study of Nevis Ta data. Before 1968 we used an electrostatic fast store, magnetic drum slow store analyzer system for data collection. It sometimes showed tendencies to add or drop data counts/channel, while the on-line computers used later were much more reliable. A cross check was thus desired for the validity of the resonances claimed from the older data before use in the Ref. 4 compilation. We also find cases when faulty arithmetic was used to convert Garg's $g\Gamma_n^0$ values to $2g\Gamma_n$ and $2g\Gamma_n^0$ values in Ref. 4. The present paper is based on measurements later than those which Rahn studied and are, thus, for different data than previously reported results.

II. EXPERIMENTAL DETAILS

The experimental details of the synchrocyclotron operation, the 202.05 m flight path, and the time of flight analyzer system are described in our earlier papers.[2] The system used 16 000 detection time of flight channels. The first 10 240 channels, above 1280 eV used 40 ns detection channel widths, increasing to 80 ns to 888 eV, 160 ns to 499 eV, 320 ns to 210 eV, 640 ns to 80 eV, and 1280 ns to 15 eV. Below 2 keV adjacent channel energy spacings were always <0.6 eV, and were <0.02 eV at 20 eV.

Counting periods of 0.5×10^6, 0.3×10^6, and 0.3×10^6 cyclotron bursts, respectively, were used for natural metallic Ta samples having $1/n = 16.6$, 79.2, and 356 b/atom in transmission, during which about 3.5×10^7 detection counts were ob-

tained in each case. A number of runs were also made using our 40 m capture detector with a $1/n = 79.2$ b/atom Ta sample at the detector, but these data did not add significantly to the analysis and were not used in our final analysis.

The analysis used the count rates at numerous "bottoming transmission dips" ($T \approx 0$) for the thick and medium samples to evaluate their background subtractions at those energies. The ratio of thick to medium sample background subtracted count rates in the transmission recovery regions near bottoming dips gave the transmission for the difference thickness. From these the implied T values for the thick, medium, and thin samples at those energies could be evaluated. This also establishes the proper thin sample background subtraction and background subtracted "open" count rates at these energies. These background subtractions and "open" rates vs energy were fitted to smooth functions of the energy suitable for the region below about 2 to 3 keV. Then E, T, and σ values were obtained for each channel and sample thickness over the energy region to a few keV above the region for which resonances were finally analyzed.

A resonance analysis for $g\Gamma_n^0$ values was first carried out using our standard "area" methods[2] and subsequently using partial shape fitting methods. The final analysis used a detailed shape fitting of the experimental T vs E using a multilevel Breit-Wigner resonance analysis which included resonance-potential interference terms from many levels at each energy, with Doppler broadening included and using a simulated resolution broadening procedure for the final computed fit curves. Distant resonances were included if they gave ≥ 0.1 b contribution to the resonance-potential interference terms at the given energy. In general, we did not attempt to distinguish between $J = 3$ and $J = 4$ for s levels since resonance and resonance-potential scattering interference terms are defined by $g\Gamma_n$, Γ, and the effective potential scattering radius R'. In a few cases, it was necessary to include resonance-resonance scattering interference to obtain a greatly improved off-resonance fit. In such cases, we do not specify the common J for the two interfering resonances. The analysis assumed a common $\Gamma_\gamma = 55$ meV for each resonance, using $\Gamma = \Gamma_\gamma + 2g\Gamma_n$.

The Γ_γ values shown in Ref. 4 suggest $\langle \Gamma_\gamma \rangle \approx 55$ MeV in agreement with our more detailed analysis for many lower energy Ta resonances.

In the final stages of the analysis, the energy interval was broken into 22 separate intervals with different best fit R' values for each interval ranging from 8.0 fm below 29 eV to 8.6 fm for some of the highest energy intervals. The increase in best R' with E relates to the positive contributions of lower energy resonances to the effective R' which are not included due to our test cutoff requirements which limit the number of interfering levels at each energy.

III. DISCUSSION OF RESULTS

The final choice resonance parameters are listed in Table I. Figures 1(a)–1(f) show (very reduced size) examples of the experimental T values and the fitting curves. Above 120 eV, the experimental points are single channel values. Below 120 eV multichannel averages were made in a selective way that did not significantly distort the resonance shapes, but reduced the statistical fluctuations and point clutter which would have resulted from the inclusion of 2000 data channels below 106 eV and 1000 channels below 35 eV. The main emphasis in choosing $g\Gamma_n$ values was on the recovery portions of the experimental transmission dips where resolution effects are less important than at the dip bottoms. The statistical accuracy of the thick sample T values was considerably better than for the thinner samples and was given greater weighting in the choice of resonance parameters.

Figure 1(a) for the 15 to 29 eV region requires two comments. The thick and medium samples show small dips in T near 18.8 eV. A weak level was listed at 18.6 eV with $g\Gamma_n = 0.4$ meV in the 1966 edition of Ref. 4, but not in later editions. We do not know the source of this dip in our thick and medium sample T values, but conclude that it is not due to Ta since the dip is larger for the five times thinner medium sample than for the thick sample. Also, it is absent in the capture data where it should have been seen if real. We were also concerned about the resonance at 20.29 eV. In the 1966 edition of Ref. 4, $g\Gamma_n$ values are reported for this resonance by seven different groups with values between about 0.54 and 0.61 meV, while our analysis gave $g\Gamma_n = 0.45$ and poor fits for $g\Gamma_n \geq 0.50$ including the recommended value (0.575 ± 0.02) meV of Ref. 4.

Figure 1(b) for $29 \leq E \leq 60$ eV clearly shows a weak resonance at 34.19 eV which has not been previously reported. It was also clearly evident in the capture data. We include resonance-potential scattering interference but usually not resonance-resonance interference since a single R' is used at each energy and resonance J values are not specified. This means that we cannot fit between resonance behavior perefectly over each entire interval. In earlier trials corresponding to Fig. 1(b), it was evident that a 35.90 and 39.12 eV resonance-resonance interference must be included to avoid extremely poor agreement in the 37 to 38 eV

TABLE I. Resonance energies and $g\Gamma_n^0$ values for ^{181}Ta resonances to 2025 eV. The fractional uncertainties in the energies are ≈0.1%, in the $g\Gamma_n^0 \approx 10\%$. The first three resonances are from BNL-325.

E (eV)	$g\Gamma_n^0$ (meV)	E (eV)	$g\Gamma_n^0$ (meV)	E (eV)	$g\Gamma_n^0$ (meV)	E (eV)	$g\Gamma_n^0$ (meV)	E (eV)	$g\Gamma_n^0$ (meV)
4.28	1.06	219.7	0.51	434.0	0.62	678.0	0.23	910.6	0.023
10.34	0.63	222.2	0.094	439.1	1.34	680.6	1.07	912.8	1.56
13.95	0.153	225.1	0.80	443.0	0.38	696.0	1.06	915.4	0.69
20.29	0.100	230.5	0.72	443.8	1.42	699.9	0.038	919.2	0.86
22.72	0.021	232.2	1.71	446.0	1.23	702.5	0.42	923.3	0.023
23.92	0.59	237.2	0.046	449.4	0.26	704.5	0.023	925.5	1.12
30.02	0.025	242.6	0.30	461.3	1.07	706.5	2.03	929.7	2.10
34.19	0.0162	247.1	0.191	465.0	0.135	710.2	0.150	931.7	1.44
35.14	1.35	248.2	0.064	467.5	2.08	716.0	2.24	936.8	0.131
35.90	1.34	252.8	0.0088	471.4	1.01	719.9	0.011	942.2	2.54
39.12	3.84	259.0	0.28	473.3	0.037	729.2	0.48	945.2	2.9
49.13	0.071	259.8	0.050	482.1	0.41	731.9	2.92	947.7	2.27
57.53	0.0185	263.1	1.48	483.4	0.205	735.7	0.74	952.2	0.54
59.05	0.0085	264.5	0.33	489.9	0.99	739.2	2.10	956.1	0.78
63.11	0.34	271.6	0.35	493.7	0.21	747.3	1.17	964.8	0.45
76.85	0.68	273.6	2.78	495.0	0.21	755.6	0.055	966.3	0.97
77.61	0.28	277.1	0.90	497.1	0.031	757.4	1.24	968.5	0.53
78.89	0.084	280.1	0.51	499.8	0.094	760.4	0.33	973.6	1.03
82.92	0.75	280.8	0.042	501.7	1.43	769.1	0.130	982.4	0.40
85.10	0.23	287.5	0.65	519.1	0.41	776.7	1.08	983.2	0.49
85.60	0.0162	290.2	0.46	552.6	2.23	781.0	0.018	985.8	0.041
89.58	0.169	291.1	0.35	524.4	0.19	782.5	0.061	988.9	0.153
91.40	0.120	304.0	0.149	527.3	2.00	789.1	1.03	993.6	0.48
96.98	0.193	306.0	0.69	533.7	1.26	797.5	0.64	996.1	0.73
99.20	6.02	311.5	0.40	536.0	0.35	800.3	0.012	1001.7	1.04
103.48	0.044	313.0	1.58	542.3	1.03	805.2	0.088	1006.3	0.21
105.53	1.36	322.7	0.156	548.8	0.35	808.2	1.16	1008.2	0.041
115.08	1.96	327.4	0.069	554.1	0.115	811.1	0.028	1015.8	0.66
118.30	0.120	328.3	0.138	556.8	1.06	813.1	2.17	1018.7	0.66
126.46	1.96	329.2	1.21	561.0	0.38	816.4	0.070	1025.5	0.23
136.45	1.03	341.3	0.168	567.0	0.097	820.8	2.09	1031.0	0.25
138.38	0.51	344.3	0.67	569.3	1.05	825.5	0.35	1033.3	0.72
144.24	0.75	346.5	0.48	576.0	0.113	830.3	0.035	1035.6	4.66
148.35	0.189	349.0	0.75	588.4	0.017	833.2	1.07	1043.1	2.29
149.80	0.229	354.1	0.88	591.3	1.15	845.7	0.31	1052.4	0.025
157.20	0.0024	357.2	0.100	596.1	6.96	874.0	0.31	1055.7	0.52
159.78	0.0095	370.1	0.99	597.0	1.84	852.5	0.82	1063.5	0.89
166.38	0.33	377.3	0.030	605.8	0.171	862.2	0.014	1071.1	2.60
174.90	4.1	378.3	0.30	608.6	0.69	869.8	0.24	1073.3	0.55
175.73	1.66	379.3	0.128	617.4	1.37	870.8	0.20	1078.4	0.27
178.54	0.049	382.0	0.021	624.2	0.64	874.0	0.91	1080.2	1.40
182.56	0.028	388.7	0.56	626.3	2.32	878.9	0.94	1082.2	0.67
185.50	0.020	396.5	0.37	635.9	0.111	881.0	0.29	1090.3	2.18
189.25	0.022	397.5	0.75	644.8	0.150	886.7	0.067	1093.5	0.45
194.76	4.01	409.8	2.08	647.4	1.57	888.5	0.181	1096.8	1.45
200.0	1.28	415.8	1.42	651.1	1.72	892.0	0.027	1102.0	0.021
204.6	0.091	416.6	1.67	658.0	0.183	894.7	0.97	1103.5	0.136
208.4	0.39	419.8	0.034	666.7	0.194	897.0	0.53	1106.3	0.024
215.0	1.77	421.7	0.063	668.4	0.128	907.0	0.103	1112.7	0.78
216.6	0.61	428.7	0.174	674.8	0.065	908.5	1.19	1119.2	0.20

TABLE I. (*Continued*)

E (eV)	$g\Gamma_n^0$ (meV)	E (eV)	$g\Gamma_n^0$ (meV)	E (eV)	$g\Gamma_n^0$ (meV)	E (eV)	$g\Gamma_n^0$ (meV)
1130.8	1.58	1362.3	1.35	1607.6	1.50	1843.5	0.82
1132.1	0.89	1364.0	1.44	1614.4	0.25	1847.4	0.140
1138.3	0.23	1372.0	0.35	1616.5	1.32	1853.5	1.72
1145.0	1.57	1376.9	1.48	1622.6	0.62	1865.1	1.39
1151.0	2.92	1378.4	0.135	1623.7	0.36	1875.8	2.08
1157.0	0.76	1387.9	0.64	1625.3	0.32	1886.4	1.98
1165.0	1.47	1391.3	2.01	1629.9	0.33	1891.3	0.97
1174.8	2.39	1398.2	2.94	1637.0	0.28	1901.7	0.48
1178.2	3.20	1408.8	0.120	1646.0	0.086	1908.6	0.062
1180.2	0.29	1409.8	0.120	1648.2	1.75	1910.2	0.144
1191.5	10.1	1413.9	0.027	1650.1	0.099	1916.0	0.050
1203.7	0.37	1417.4	0.27	1652.0	0.71	1928.1	1.23
1208.5	0.35	1426.5	0.26	1655.1	1.87	1931.4	0.114
1211.8	0.30	1430.7	1.72	1664.3	0.123	1933.4	1.25
1216.1	0.072	1437.4	0.053	1667.0	0.029	1936.3	0.193
1218.6	0.49	1440.9	0.145	1670.2	1.13	1939.2	0.091
1220.7	0.186	1443.8	0.25	1673.4	0.95	1941.2	0.55
1226.6	1.37	1450.5	0.87	1677.8	1.68	1944.6	0.54
1232.7	0.142	1455.2	0.37	1681.0	0.22	1949.8	1.11
1239.9	0.31	1463.4	0.094	1692.0	0.92	1958.9	0.25
1246.1	1.30	1465.3	0.23	1696.7	4.03	1964.1	0.68
1247.8	1.13	1468.7	0.23	1698.8	0.85	1969.7	0.32
1252.2	0.028	1470.9	0.094	1701.8	0.061	1970.7	0.135
1259.1	1.35	1473.3	0.039	1704.2	0.24	1982.6	0.124
1261.2	0.037	1475.2	1.87	1708.9	0.036	1988.8	0.370
1263.1	0.62	1490.4	0.093	1713.0	0.97	1995.7	0.184
1267.9	0.169	1494.6	0.036	1719.7	0.58	1998.0	1.45
1275.7	1.48	1501.5	0.67	1720.7	0.36	2001.2	0.38
1280.2	0.98	1508.2	0.52	1724.5	0.039	2004.6	0.179
1283.1	0.36	1512.8	0.026	1728.0	0.168	2011.6	0.067
1286.8	0.34	1517.4	2.05	1731.3	0.44	2014.3	2.23
1291.4	0.39	1591.9	1.28	1732.5	1.83	2017.6	1.78
1293.3	1.11	1522.9	3.33	1734.3	1.92	2020.0	1.11
1299.7	2.50	1525.0	0.15	1735.9	2.42	2023.2	0.78
1307.1	0.22	1531.5	0.77	1741.6	1.85		
1311.0	0.069	1537.3	0.26	1743.4	0.58		
1312.7	1.19	1541.0	0.23	1751.0	1.89		
1317.0	1.02	1546.9	0.064	1766.7	0.69		
1323.5	0.179	1554.6	1.07	1769.7	0.52		
1327.0	0.137	1555.9	1.65	1784.2	0.24		
1328.6	2.41	1565.1	1.69	1792.4	0.37		
1332.2	2.47	1571.0	0.126	1796.1	0.156		
1334.0	0.21	1576.3	0.176	1800.6	1.44		
1335.3	1.10	1579.0	0.629	1808.5	0.59		
1342.3	0.123	1582.0	0.038	1810.4	0.28		
1349.4	0.068	1584.7	1.13	1821.2	0.23		
1352.1	0.22	1585.8	1.06	1829.4	0.27		
1356.3	0.027	1591.0	0.55	1835.6	0.079		
1359.1	0.098	1601.9	1.03	1838.3	0.26		
1360.6	1.17	1603.0	1.00	1841.5	0.28		

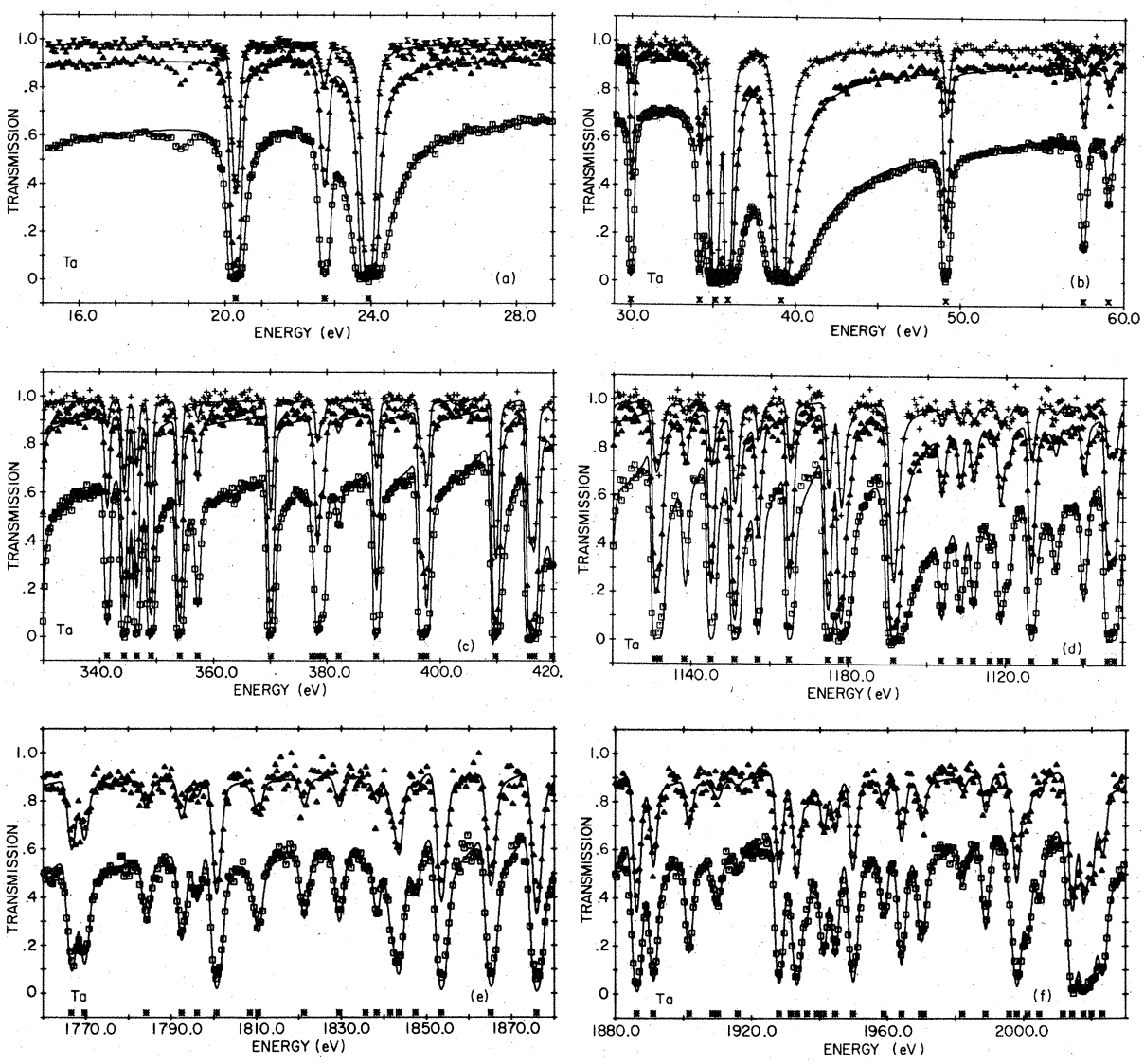

FIG. 1. Sample plots of the experimental transmission of natural Ta samples [$1/n = 356$ (top), 79.2 (middle), and 16.6 (bottom) b/atom thickness]. The curves are the final "best fit" theoretical transmission curves using a multilevel Breit-Wigner formalism, Doppler corrected, and including some simulated resolution broadening. (a) 19 to 29 eV, $R' = 8.0$ fm. (b) 29 to 60 eV, $R' = 8.1$ fm. (c) 330 to 420 eV, $R' = 8.2$ fm. (d) 1120 to 1250 eV, $R' = 8.5$ fm. (e) 1760 to 1880 eV, $R' = 8.6$ fm. (f) 1880 to 2030 eV, $R' = 8$ fm. The thinnest sample data were omitted in (e) and (f). See the text for further discussion. The E, $g\Gamma_n^0$ values used are given in Table I.

region. One would prefer a smaller R' below 39 eV and a slightly larger R' from 40 to 60 eV. Other cases where level-level interference was needed and used were by level pairs at 99.20 and 105.53 eV (which are not adjacent), at 174.90 and 194.76 eV (which have five levels intermediate), at 290.16 and 291.09 eV, at 591.33 and 596.05 eV, at 1035.60 and 1043.11 eV, and at 1078 and 1191.52 eV. In Fig. 1, note that an asterisk indicates the position of each resonance included in the fitting process.

Figure 1(c) for the 330 to 420 eV region contains 18 resonances for the theoretical fitting. In most cases, the choices are obvious. A few cases deserve further comments. The cluster of three levels near 378 eV was needed although a quick glance at the data suggests that only two poorly resolved levels are present. Very poor fitting resulted from attempts to include only two levels. The dip shapes near 397 and 416 eV need two close poorly resolved levels for a fit. The medium and thin sample calculated dips are much too narrow using single level parameters which give a best fit to the thick sample dip. The recovery regions are also

poorly fitted. Garg[4] had used one less level near 377 eV, but also two each near 397 and 416 eV.

Figure 1(d) shows the region 1120 to 1250 eV where 22 levels were used for the theoretical fitting. This region contains the strongest ($g\Gamma_n$ or $g\Gamma_n^0$) resonance in the $E=0$ to 2030 eV range studied. It is at 1191.52 eV and dominates a region ~10 eV wide. The level at 1178.15 eV is also one of the strongest levels. While we could have fitted the dip near 1192 eV using two or more levels, there did not seem to be strong enough justification for doing so even though for $\langle S\rangle \sim 4.2$ eV, one expects several levels to occur between the levels at 1180 and 1204 eV. The dip near 1178 to 1182 eV did require an additional weak level at 1180.20 eV which was not included in Garg's analysis.

The comparison of the experimental distribution of $(g\Gamma_n^0)^{1/2}$ values with a single channel Porter-Thomas fit indicates that the $g\Gamma_n^0$ value for the 1191 eV level is improbably large. The breakdown into two or more separate resonances could only be made in an arbitrary way, however.

Figure 1(e) for 1760 to 1880 eV shows a region where the analysis is relatively simple. Figure 1(f) for 1880 to 2030 eV contains the very complicated structure between 2010 and 2030 eV which required five levels to obtain the fit shown. The analysis of this region discouraged attempts to continue to higher energy, where the situation became even worse. The lower energy data implies a mean level spacing $\langle S\rangle$ of about 4.2 eV. There is no level repulsion between levels of different J, so we expect to miss an increasing fraction of weak or overlapping levels at higher energies. Our level energies and $g\Gamma_n^0$ values are in reasonable agreement with those of Garg[4] to 1400 eV, but are considered to be more reliable. We would restore a number of Garg's levels which were omitted from Ref. 4 because Rahn could not "see" evidence for them in our 1968 data. We would still continue to delete many of his very weak "levels" which were probable statistical fluctuation effects in the earlier Nevis data.

Figure 2 gives a plot of the cumulative level count N vs energy. Above 600 eV the slope seems to decrease somewhat, but it does not show a continuing large decrease of the type usually seen. This is probably due to the unresolved levels required in our fitting process. Below 600 eV a mean level spacing of about 4.30 eV is indicated, and 4.6 eV above 600 eV.

Missing weak levels do not influence $\sum g\Gamma_n^0$ significantly so Fig. 3 is expected to be less perturbed than Fig. 2 by missed levels. The slope of this curve determines the $l=0$ strength function S_0. A value $10^4S_0=1.70$ gives a fit going alternately above and below the histogram over the entire energy region. Using $\sum g\Gamma_n^0/\Delta E$ gives $10^4S_0=1.68$, where $\Delta E=2023$ eV. Using the conventional statistical choice $\Delta S_0/S_0=(2/N)^{1/2}$ for the fractional uncertainty in S_0 and $N\approx 486$ gives $10^4S_0=(1.68\pm 0.11)$ eV. This neglects uncertainties in the individual $(g\Gamma_n^0)$ values and possible differences in $\langle g\Gamma_n^0\rangle$ for the $J=3$ and 4 level populations. The three slopes are shown in Fig. 3.

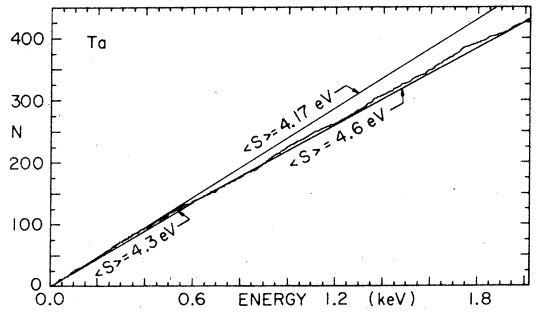

FIG. 2. Plot of cumulative level count, N vs E. The experimental curve slopes $\langle S\rangle=4.3$ to 600 eV and $\langle S\rangle=4.6$ eV above 600 eV are shown. The deduced $\langle S\rangle=4.17$ eV curve is also shown. This estimates the contribution of missed $l=0$ levels.

Figure 4 gives a histogram of $(g\Gamma_n^0)^{1/2}$ for the energy intervals 0–600, 0–1000, and 0–2025 eV. For each $(g\Gamma_n^0)^{1/2}$ interval, the histogram heights increase as $E_{\max}$ increases, unless there are overlaps. The $\Delta(g\Gamma_n^0)^{1/2}$ box widths are all 0.10 $(\text{meV})^{1/2}$. A comparison single channel Porter-Thomas (PT) Gaussian fit is given which is based on $10^4S_0=1.70$ and using $N=144$, 240, and 486 for the three energy regions, respectively, compared with $N=137$, 224, and 434 levels observed. The last level contributing to the first box, $0\leq g\Gamma_n^0\leq 0.01$ meV is at 252.8 eV. Clearly we missed an increasing number of levels for this box as $E_{\max}$

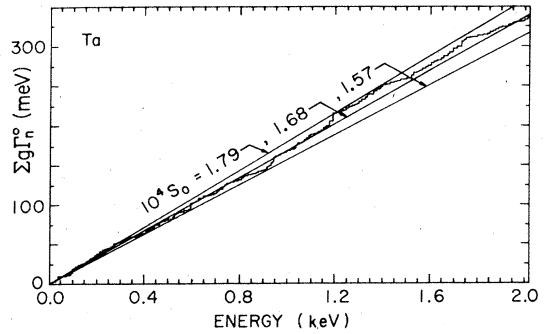

FIG. 3. Plot of $\sum g\Gamma_n^0$ vs energy. The slope is the implied $l=0$ strength function. It is relatively insensitive to missed weak $l=0$ resonances. The three straight line slopes are for $10^4S_0=(1.68\pm 0.11)$ where the fractional uncertainty is due only to statistical sample size for a single channel Porter-Thomas distribution of reduced widths.

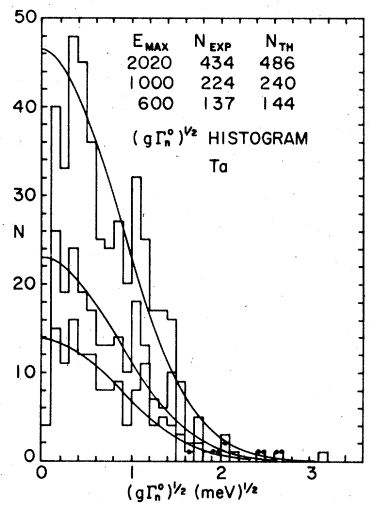

FIG. 4. Histogram of $(g\Gamma_n^0)^{1/2}$ values for the energy intervals 0–600, 0–1000, and 0–2025 eV. The theoretical Porter-Thomas fit curves are for the same $\langle g\Gamma_n^0\rangle$ for the two compound nucleus spin states, and are for $10^4S_0=1.70$, $\langle S\rangle=4.17$ eV. From this figure estimates of the number of missed $l=0$ resonances are made in the text. One dot on a nonzero bar indicates that it occurs twice, and two dots that it occurs three times.

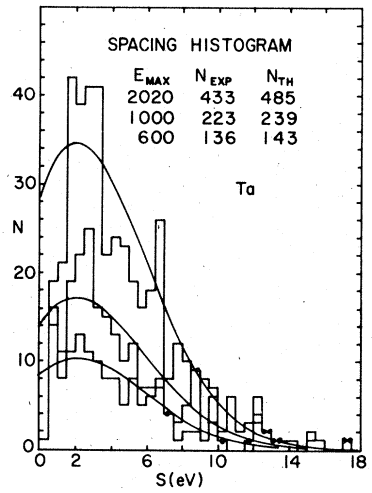

FIG. 5. Histogram of observed nearest neighbor level spacings 0–600, 0–1000, and 0–2025 eV. Since two nearly equal density merged level populations ($J=3$ and 4) are present, the theoretical Wigner distribution curves are for that case. The absence of level repulsion and finite experimental resolution lead to many cases of unresolved resonances, as discussed in the text. One dot on a nonzero bar indicates that it occurs twice, and two dots that it occurs three times.

increases. The second box is for $0.01 \leq g\Gamma_n^0 \leq 0.04$ meV. The last contribution to this box is by the 1724.5 eV level. We seem to miss levels corresponding to this box above 1 keV. The Porter-Thomas fit to 1000 eV suggests that about 15–18 levels having $g\Gamma_n^0 < 0.01$ meV are missed. The value 15 deducts for extra levels in the second box. A count of 240 resonances is chosen as correct for the true number to 1000 eV, corresponding to a mean level spacing $\langle S\rangle = 4.17$ eV, 486 resonances to 2025 eV, and 144 resonances to 600 eV. The fit suggests that we also missed some resonances from the second and third histogram box in going from 1000 to 2025 eV. The fits are otherwise within statistical fluctuations except for the two or three strongest levels ($g\Gamma_n^0$ values). In fact, the comparison of the histogram to 2025 eV with the PT fit seems to indicate that the strongest resonance at 1191.52 eV should be broken up into two or more resonances. The next strongest level at 596 eV also has an improbably large $g\Gamma_n^0 = 6.96$ meV in the fit 0 to 1000 eV.

The histogram distribution of nearest neighbor level spacings is shown in Fig. 5 for the energy intervals 0–600, 0–1000, and 0–2025 eV. The comparison curves are the expected form for two randomly merged Wigner distributions having relative level densities proportional to $(2J+1)$ for $J=3$ and 4. It is seen that there are too few values of $S<0.5$ eV to 600 eV and to 1000 eV. The distribution to 2025 eV also has a shortage of small spacings in the second and third histogram boxes with an excess for the next four intervals and an improbably large number of spacings ≥ 15 eV. We did not expect to have good agreement with theory because of the increasing probability of missing weak levels and not resolving close levels as E increases.

A study of the threshold $g\Gamma_n$ vs E for level detection suggested a threshold such that levels would be missed when $g\Gamma_n < 1.6\times10^{-5}\,(E/1\text{ eV})^{1.5}$ meV. For $\langle S\rangle = 4.2$ eV and $10^4S_0 = 1.7$, the Porter-Thomas distribution of $g\Gamma_n^0$ values suggested that ~18 s levels would be missed to 1000 eV and ~52 levels to 2000 eV. It also showed that $10^4S_1 \gtrsim 0.6$ was required before one or more p levels would be included to 2000 eV assuming a p level density 2 times the s level density from the statistical factor. A Bayes theorem analysis for the probability of each resonance being $l=0$ or $l=1$ using $10^4S_0 = 1.7$, $\langle S\rangle = 4.2$ eV, vs trial values for 10^4S_1, gave a net weighted probability that two of our levels in Table I were $l=1$ for $10^4S_1 = 0.6$, increasing to 4 or 5 for $10^4S_1 = 0.75$. The plot, on page xxii at the front of Ref. 4, of S_1 vs A suggests that $10^4S_1 = 0.3$ for ^{181}Ta, so one expects that none of our reported levels are p wave.

Our value $10^4S_0 = (1.68 \pm 0.11)$ for ^{181}Ta is in satisfactory agreement with the recommended value (1.8 ± 0.2) of Ref. 4, which is based mainly on

Garg's analysis to 1400 eV of the older Nevis data. Desjardins *et al.*[3] had obtained $10^4 S_0 = (1.84 \pm 0.34)$ from the early Nevis self-indication data on 62 resonances to 330 eV, while we would now assign 1.73 for this interval. A comparison of our $g\Gamma_n$ values with those of Ref. 4 shows reasonable agreement in most cases, with about half of our values slightly larger than the reference values. There are some levels, such as at 313 eV, where the reference values (Garg's) are about twice ours. We suspect factors of 2 arithmetic errors in these cases for his values.

Our final choice for $\langle S \rangle$ is (4.17 ± 0.04) eV as the estimated uncertainty.

This research was supported by the U. S. Energy Research Development Administration and the National Science Foundation.

---

*Present address: Decision Systems, Inc., 200 Route 17, Mahwah, New Jersey 07430.

[1]G. Hacken, J. Rainwater, H. I. Liou, and U. N. Singh, Phys. Rev. C 13, 1884 (1976), ^{139}La.

[2]References to all previous papers in this series can be found in U. N. Singh, J. Rainwater, H. I. Liou, G. Hacken, and J. B. Garg, Phys. Rev. C 13, 124 (1976), ^{209}Bi.

[3]J. S. Desjardins, J. L. Rosen, W. W. Havens, Jr., and J. Rainwater, Phys. Rev. 120, 2214 (1960).

[4]*Neutron Cross Sections*, compiled by S. F. Mughabghab and D. I. Garber, Brookhaven National Laboratory Report No. BNL-325 (National Technical Information Service, Springfield, Virginia, 1973), 3rd ed., Vol. I, Resonance Parameters.